Curvature and Orientation Estimation by Neuronal Structures

Júlia Sawaki Tanaka[1,2], Edson Tadeu Monteiro Manoel[1], Luciano da Fontoura Costa[1]

[1] Cybernetic Vision Research Group – University of São Paulo
Caixa Postal 369, CEP 13.560-970, São Carlos, SP, Brazil
e-mail: {julia, luciano}@if.sc.usp.br; emanoel@icmc.sc.usp.br

[2] DFQ – IQ – UNESP – Caixa Postal 355, CEP 14.801-970, Araraquara, SP, Brazil
e-mail: julia@iq.unesp.br

Abstract. It is presented a simple model of curvature and orientation estimation by neuronal networks where a pair of neurons is used to approximate the partial differential operators needed for curvature and orientation estimation. The influence of neuronal morphometry in the estimation of curvature and orientation is investigated and discussed. In addition, the biological plausibility of the model is discussed, and simulation results are presented along a sequence of increasing plausibility and sophistication. Steerable filters are considered as a means to increase the model efficiency.

1 Introduction

The representation of the curves such as shape contours is an important problem in computer vision because of the special human ability to recognize objects represented in terms of their 2D contours, even without information about depth, color or texture. Because of its special importance, the human perception of curvature and orientation have been investigated for a long time [2, 11, 16], but no definitive conclusion about specific operators for curvature estimation has been reached. As far as orientation is concerned, there are conclusive results indicating what kind of cells and respective receptive fields are involved in this task. Some studies have indicated that the performance of curvature discrimination is influenced by other features such as orientation [9, 14, 17], length [8, 17, 18], blur and contrast [19]. While there are studies suggesting the existence of curvature detectors, i.e. neurons specific to curvature estimation [1, 15, 17], other studies suggest that curvature is processed by integrating information about different orientations [2, 20]. Lehky and Sejnowski [13] constructed a neural network model to determine curvature of simple geometric surfaces, incorporating only the gray level image of the surface. Their model uses a three-layer network trained by backpropagation.

In order to investigate a possible model to perform curvature and orientation estimation, we propose an approach based on partial differential operators that presents biological plausibility. A preliminar description of the model has been presented in references [5, 7]. In this work, we present an extension of the model to allow biologically more realistic simulations and the use of steerable filters to increase the efficiency of the model. Also presented are some neuromorphometric features to evaluate the relation between neural shape and function, specifically in curvature and orientation estimation.

2 Curvature and Orientation Estimation Model

The model is based on partial derivative operators, $\phi_x = \partial\phi/\partial x$ and $\phi_y = \partial\phi/\partial y$, from which the gradient Equation 1 and curvature Equation 2 are obtained.

$$\vec{\nabla}\phi = \phi_x i + \phi_y j \qquad (1)$$

$$k = \vec{\nabla} \cdot \frac{\vec{\nabla}\phi}{\left\|\vec{\nabla}\phi\right\|} \qquad (2)$$

We use as a stimuli a closed contour extended into a surface $\phi(x, y)$ in such a way that internal points are represented as one and external points as zero. The Equation 2 provides the 2D curvature along each level curve of the surface. The orientation was considered as the angle formed by the gradient vector and the positive x-axis direction, counterclockwise, ranging between 0 and π radians.

We proposed a neural network structure capable of estimating the partial derivative operators by taking into account the electrotonic decay[1] along the neurons dendrites. In this model, all synaptic efficiencies are similar, in such a way that their effective weights are determined by the electrotonic decay, approximated by an exponential, which is the steady-state solution of the passive transmission cable [12]. Therefore, the further the synapse is from the soma, smaller is its influence on the neuron discharge. The efficiency of the synapse is given

[1] electrotonic decay is the decrease of synaptic potential along the dendritic process .

0-7695-0878-2/00 $10.00 © 2000 IEEE

by $\varepsilon = e^{-s/\alpha}$, where s is de arc length distance between the synapse and the soma.

The basic idea in this model is to use de planar neural shape as a correlation mask (template), so that the activity of the cells are determined by the internal product between the weights template and the input stimulus (image). When the mask is a Gaussian smoothed partial derivative operator ($\partial/\partial x$), as illustrated in the Figure 1(a), the result of the correlation between the mask and the image is a scalar field corresponding to ϕ_x. The Gaussian smoothing is used to reduce the noise generated by the sampled representation of the stimulus.

As it can be seen in the Figure 1(a), it is necessary both positive and negative weights to approximate the Gaussian smoothed partial derivative mask. We considered two neurons, one representing the excitatory synapse and another the inhibitory synapse. A small distance δ separates these two neurons.

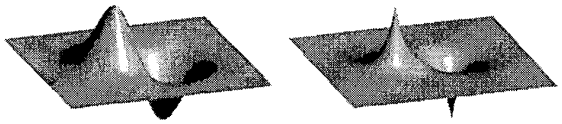

(a) (b)

Figure 1 – (a) Gaussian smoothed $\partial/\partial x$ mask; (b) difference of two exponentials mask.

The weights of the neurons of the mask, defined by electrotonic decay along their dendrites are given as:

$$E_\alpha(x,y) = \beta \exp\left\{-\frac{1}{\alpha}\sqrt{x^2+y^2}\right\} \qquad (3)$$

where β is a proportionality coefficient and α is the parameter that controls the width of the exponential.

Leaving the neurons aside, we can construct a mask considering the differences of two exponentials (*DOE*), Figure 1(b), given by the following equation:

$$DOE_{\alpha,\delta}(x,y) = \beta\left(\exp\left\{-\frac{1}{\alpha}\sqrt{\left(x+\frac{\delta}{2}\right)^2+y^2}\right\} - \exp\left\{-\frac{1}{\alpha}\sqrt{\left(x-\frac{\delta}{2}\right)^2+y^2}\right\}\right) \qquad (4)$$

As it will be illustrated in the paper, the correlation between this mask and the image can approximate the partial derivative ϕ_x of the image.

In the next section we present the results of simulations starting with the use of *DOE* mask and following with a sequence of increasingly more biologically plausible extensions.

3 Neuromorphometric Features

The study of relation between cell shape and function on neural information processing [4, 6, 7] is a particularly important issue that has received relatively little attention. This section presents 4 morphological features of the cell that reflect its geometry and important characteristics affecting curvature and orientation estimation.

3.1 Complexity

The complexity of the shape can be measured by fractal dimension. First we obtain the dilation of the shape by using Minkowski sausage method. Next, the log-log graph of the Minkowski sausage radius against the area of the dilation is obtained, and the fractal dimension is approximated by 2–s, where s is the slope of the log-log plot. Here an improved method described in reference [3] was adopted in order to compute the fractal dimension.

3.2 Curvature

A morphologically important measure of a cell is the curvature of their processes. The curvature is calculated at each contour point of the processes, in such a way that a small curvature value indicates the local straightness of the process.

3.3 Radiality

Radiality measures how much the processes of the cell are radially organized around the center of mass of the soma. For each contour point of the process the angle between the tangent vector in that point and the radial direction is calculated, see Figure 2. So, the smaller the angle, the more locally radial that point is.

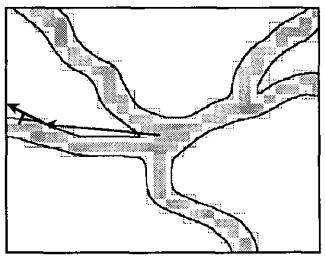

Figure 2 – Geometric construction considered for the radiality measure.

3.4 Radial Symmetry

A measure that quantifies the radial distribution of the cell processes is the radial symmetry. The angle between the segment (which connects a point of the process and the center of mass of the soma) and the positive x-axis is calculated. A uniform distribution of these angles between 0 and 2π radians indicates that the processes are radially

distributed and, consequently, that the cell presents radial symmetry.

4 Simulations

We used the parameter $\beta = 1$ and searched for parameters δ and α that best approximate the partial derivative operators. The parameter δ was varied with step 1 and the parameter α with step 0.1, and the parameters allowing the minor overall error (E), given by Equation 5, were identified.

$$E = \frac{1}{M}\sum_{i=1}^{M}\left|C_i - \tilde{C}_i\right| \qquad (5)$$

Observe that M is the number of points where the standard curvature (C) is not null, and $\tilde{C}$ is the approximated curvature. The standard and approximated curvature and orientation are obtained by using the sian smoothed partial derivative mask and the *DOE* mask, respectively.

The best parameters found for image size 513x513, used in these simulations, are $\delta = 14$ and $\alpha = 2.5$.

4.1 Curvature and orientation estimation using the standard partial derivative operator

Figure 3(a) presents the original synthesized shape (curve) from which the curvature and orientation is to be calculated. Figure 3(b) illustrates the shape filled to produce the surface. The curvature obtained by applying the Gaussian smoothed partial derivative operators ($\partial/\partial x$ and $\partial/\partial y$) is shown in Figure 3(c), and the Gaussian smoothed partial derivatives along x (ϕ_x) and y (ϕ_y) are shown in Figures 3(d) and 3(e). In the Figure 3(c), 3(d) and 3(e), a line is superposed to indicate the position of the curve. In the Figure 3(c) the black and white colors indicates high curvature with opposite sign. The curvature of interest is that corresponding to the points along the original contour. The used image size is 513x513 in all simulations, unless when specifically indicated.

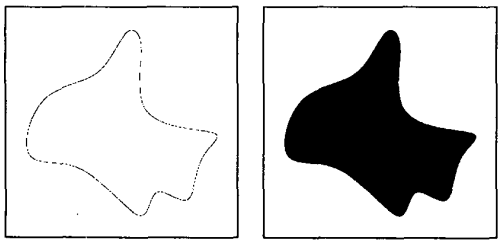

(a) (b)

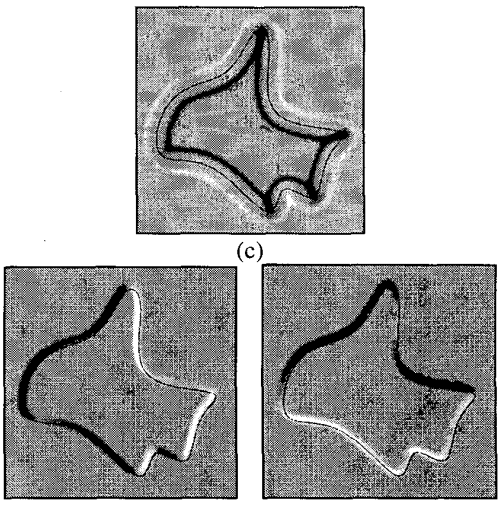

(c) (d) (e)

Figure 3 – (a) original shape; (b) filled shape; (c) curvature estimated by Gaussian smoothed $\partial/\partial x$ operator; (d) scalar field ϕ_x ; (e) scalar field ϕ_y.

4.2 Curvature and orientation estimation using the *DOE* operator

Figure 4 presents the results obtained by using the *DOE* mask with $\beta = 1$, $\delta = 14$ and $\alpha = 2.5$ and respective histograms. The error histogram is generated by taking into account the differences between the results obtained by the use of Gaussian smoothed partial derivative (standard) mask and the *DOE* mask, at the points where the standard curvature is not null.

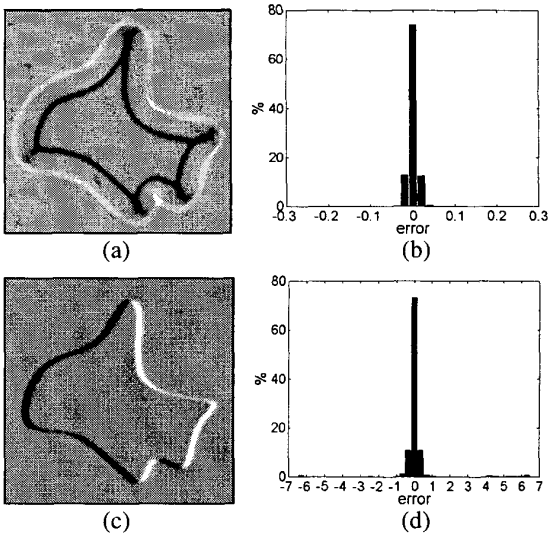

(a) (b) (c) (d)

Figure 4 – (a) estimated curvature; (b) curvature error (pixel^{-1}) histogram; (c) ϕ_x ; (d) orientation error (radians) histogram.

In the following simulations, the mask was centered at the nodes of an orthogonal lattice with parameter d. Hence, when $d = 1$ the mask is applied at each pixel of the image.

In the first series of simulations using the *DOE* mask reflecting the neural shape, the same cell was used to compose all masks, in order to investigate the influence of the cell morphology over curvature and orientation estimation.

Figure 5 illustrates 4 synthesized cells with dimension 81x81 used in this first series of simulations. The varied cell shapes were used to verify the influence of the cell geometry in the estimation. The features previously presented in section 3 were obtained from each of the cells in order to characterize its geometry. Figure 6(a) shows the complexity of the cells; Figure 6(b) and (c) present the mean and the standard deviation of the cell curvature and the cell radiality, respectively. The mean is represented by circle and the standard deviation by bar. Figure 6(d) depicts the standard deviation of the histogram of cell radial symmetry. The Figures 7(a)-(d) shows the histograms of curvature estimation error of the 4 cells and the Figures 7(e)-(h) shows the histograms of orientation estimation error calculated in radians for the 4 cells. Both curvature and orientation were obtained with $d = 1$.

Analyzing the results it is possible to verify that a complex and radially symmetric cell allows the curvature and orientation estimation to be performed in a more accurate fashion.

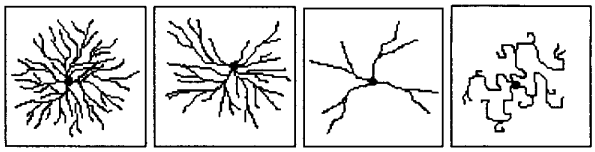

(a) (b) (c) (d)

Figure 5 – Synthesized cells used to investigate the influence of its morphometry in the curvature and orientation estimation; (a) Cell 1; (b) Cell 2; (c) Cell 3; (d) Cell 4.

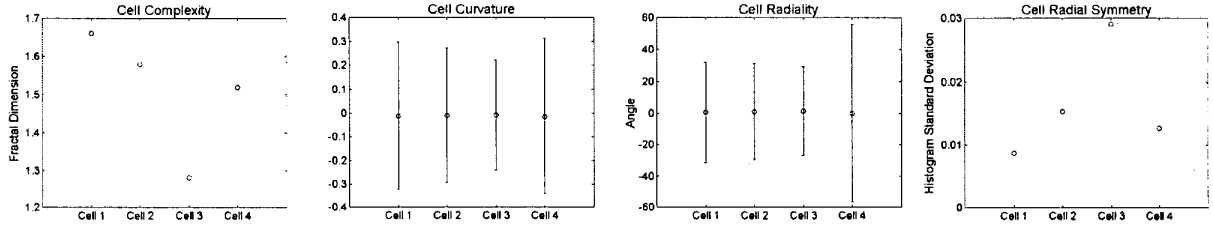

(a) (b) (c) (d)

Figure 6 – Morphometric measures of the cells; (a) cell complexity; (b) cell curvature; (c) cell radiality; (d) cell radial symmetry.

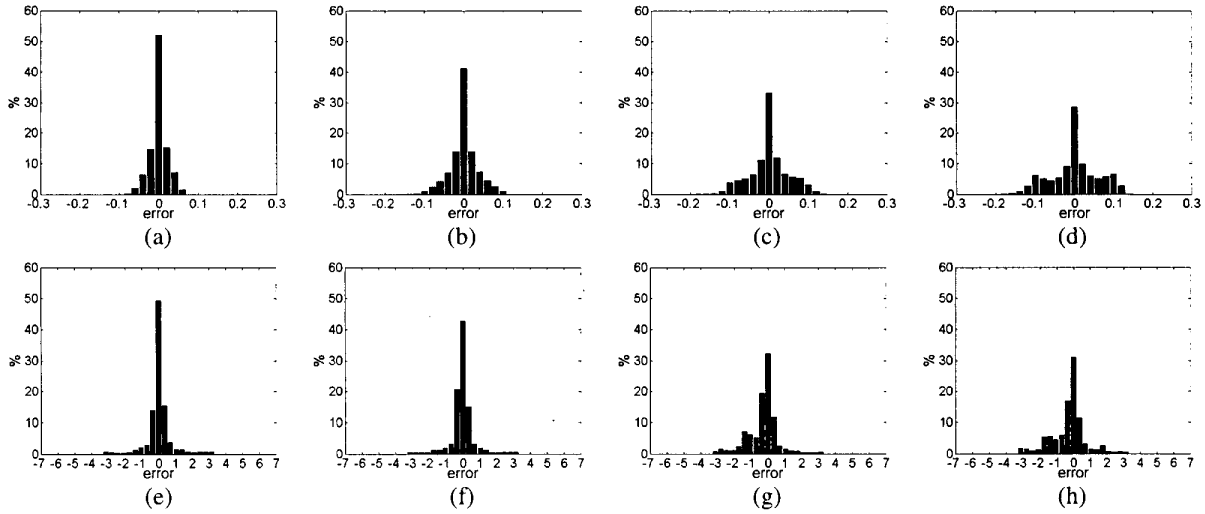

(a) (b) (c) (d)

(e) (f) (g) (h)

Figure 7 –Histogram of curvature estimation error obtained by Cell1 (a), Cell2 (b), Cell3 (c), Cell4 (d) and histogram of orientation estimation error obtained by Cell1 (e), Cell2 (f) , Cell3 (g) and Cell4 (h).

The next series of simulations consider 8 synthesized cells with dimension 81x81, illustrated in the Figure 8.

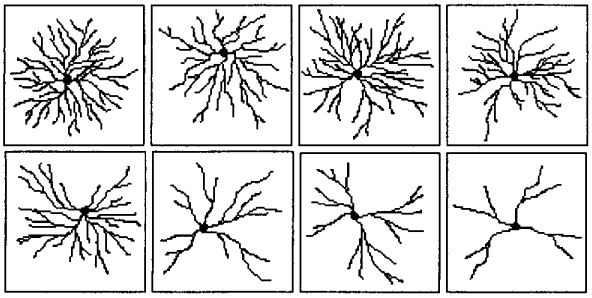

Figure 8 – Synthesized cells used in the *DOE* masks.

Now we consider randomly chosen cells of the Figure 8 to compose both the positive and negative receptive fields of each *DOE* mask used for estimating the partial derivatives. Figure 9 shows the results of this simulation using $d = 1$.

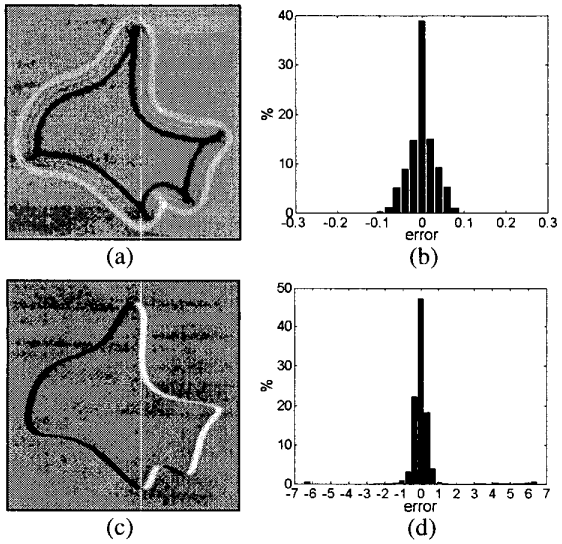

Figure 9 – (a) estimated curvature; (b) curvature error (pixel^{-1}) histogram; (c) ϕ_x ; (d) orientation error (radians) histogram.

In Figure 10 we can visualize the results obtained by using the *DOE* mask in the same conditions as before, but with $d = 3$. Here the mask is centered at a regular grid of distance 3. In the cases as this in that the mask is not applied centered at all pixels, the error is calculated only in the pixels where the mask is centered.

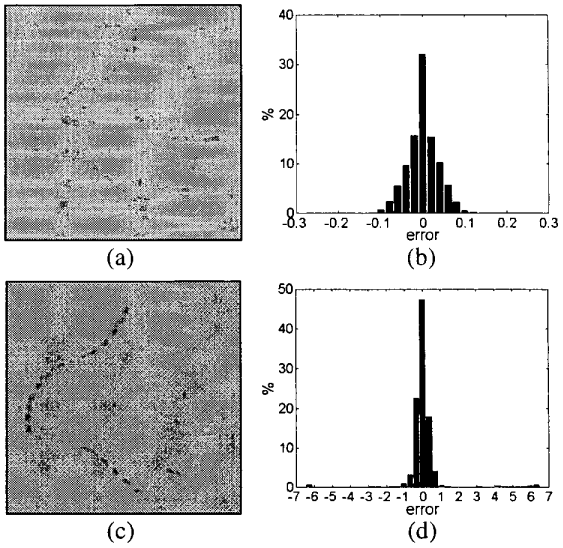

Figure 10 – (a) estimated curvature; (b) curvature error (pixel^{-1}) histogram; (c) ϕ_x ; (d) orientation error (radians) histogram.

The results obtained by using randomly selected different cells to compose the positive and negative parts of the *DOE* mask, with $d = 1$, is illustrated in the Figure 11. A degradation of the curvature and orientation obtained is verified, caused by the misbalance between the different cells composing the *DOE* mask. Even so, the results are still reasonable.

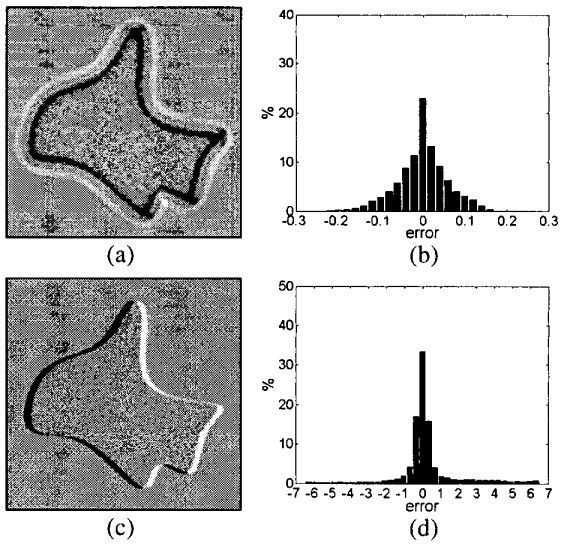

Figure 11 – (a) estimated curvature; (b) curvature error (pixel^{-1}) histogram; (c) ϕ_x ; (d) ϕ_y ; (e) orientation error (radians) histogram.

4.3 Curvature and orientation estimation using randomly positioned cells with *DOE* operator

Thus far, the simulations started with Gaussian smoothed standard partial derivative masks and proceeded to the different cells composing each of *DOE* masks, increasing the biological plausibility. In all simulations the mask was centered at a regular grid of distance *d*. Proceeding with the increase of biological plausibility, the next simulation considers random placements of cells through the input image, as illustrated in the Figure 12. First, a cell is randomly selected and another three cells of its neighborhood are chosen to form the pair of *DOE* to approximate $\partial\phi/\partial x$ and $\partial\phi/\partial y$. To form a good pair of *DOE*, the cells need to satisfy the following criteria:

- The distance between two cells of each *DOE* must be as close as possible to δ;
- The two pairs of *DOE* must form an angle the closest as possible to orthogonal angle;
- The centers of the *DOE* masks must be as close as possible.

These three criteria were considered to choose the best four cells to compose the pair of *DOE* masks, following a function that is a linear combination of the measures that express the criteria. Figure 13 shows the results of using randomly positioned cells in a 257x257 input image. The parameters used for these image size are $\delta = 6$ and $\alpha = 1.4$.

Although we can verify some degradation in the results, the model still is able to estimate curvature and orientation.

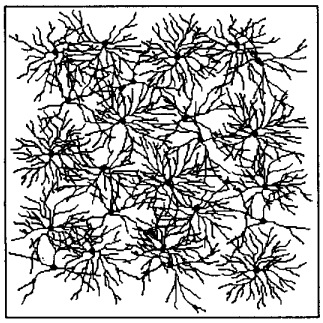

Figure 12 – Randomly placed cells.

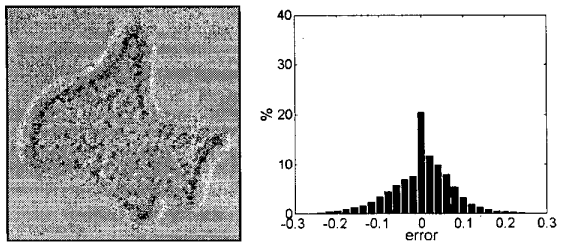

(a) (b)

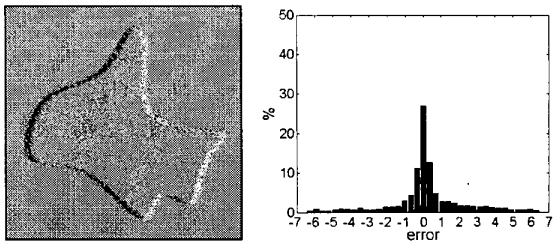

(a) (b)

Figure 13 – (a) estimated curvature; (b) curvature error (pixel^{-1}) histogram; (c) ϕ_x ; (d) orientation error (radians) histogram.

4.4 Curvature and orientation estimation using randomly positioned cells with *DOE* operator and steerable filters

Estimating the curvature and orientation in this way, i.e. by using randomly positioned cells, the angle formed between the two *DOE* masks may not be orthogonal. However, it is possible to use steerable filters [10] to improve the results.

Steerable filters are a class of filters that can synthesize an arbitrary oriented filter from linear combination of the basic filters. In this case, we have the partial derivative ϕ_x and a derivative in the direction θ other than 90°, and we want to obtain ϕ_y orthogonal with ϕ_x, as illustrated in the Figure 14.

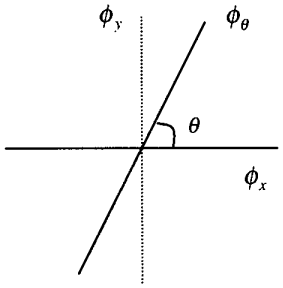

Figure 14 – The basic geometric construction used in order to improve the curvature estimation.

Starting from the steerable filter equation presented in the Equation 6, we obtain the Equation 7.

$$\phi_\theta = \cos(\theta)\phi_x + \sin(\theta)\phi_y \qquad (6)$$

$$\phi_y = \frac{1}{\sin(\theta)}\phi_\theta - \frac{1}{\mathrm{tg}(\theta)}\phi_x \qquad (7)$$

Using the Equation 7 and assuming that another cell is receiving the inputs (ϕ_θ and ϕ_x) with the respective

weights $\left(\frac{1}{\sin(\theta)} \text{ and } -\frac{1}{\mathrm{tg}(\theta)}\right)$, the results illustrated in the Figure 15 are obtained, considering the same parameters used at former simulation.

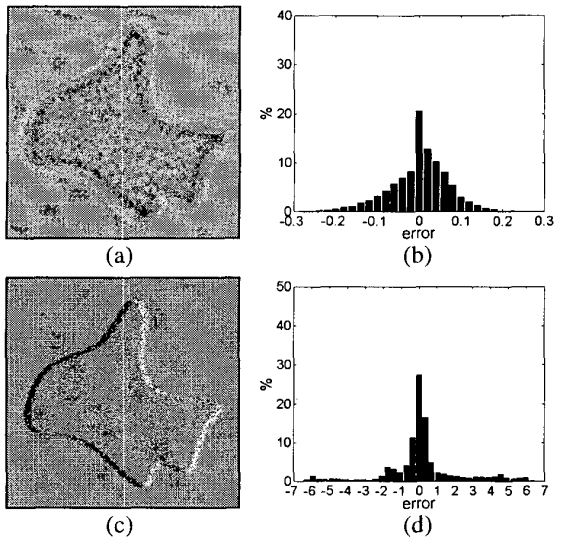

Figure 15 – (a) estimated curvature; (b) curvature error (pixel^{-1}) histogram; (c) ϕ_x ; (d) orientation error (radians) histogram.

The use of steerable filters has been verified to sensibly increase the performance of the model so much for curvature as for orientation.

As previously mentioned, the divergent of normalized gradient, obtained from Gaussian smoothed partial derivative operators, was used to be the comparison pattern for curvature and orientation estimation. To validate the curvature estimation obtained with this operators, the error histogram shown in Figure 16 is considered for comparing the curvatures obtained with these operators and the analytical curvature in the points of the considered curve of the 513x513 image. The analytical values were quantized taking the medium value of the curvatures, in order to allow comparisons with the digitized curvature.

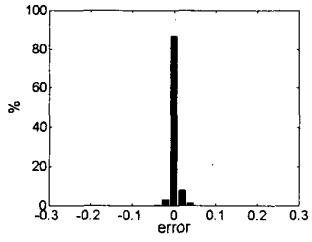

Figure 16 – Error histogram of pattern curvature in relation to the analytical curvature.

5 Conclusions

The presented model is based on the difference of two exponentials, implemented in terms of a pair of neural cells. The weights are defined in terms of electrotonic decay along the dendrites of the cells, and are consequently modeled by a decreasing exponential function of the arc length between the synapse and the soma.

The models progressed according to a sequence of increasing biological plausibility, and we verified that the accuracy of the curvature and orientation estimation was verified to decrease along this sequence. Even so, the model can still give a reasonable indication about curvature and orientation of the presented stimulus. It is also been verified that the use of steerable filters increased the efficiency of curvature and orientation estimation. The obtained results also imply that a complex cell with radially distributed processes is more suitable for curvature.

In spite of being a computational model based in a mathematical equation, electrophysiological aspects like electrotonic decay and a natural organization of the cells with random distribution have been incorporated to make the model more biologically realistic capable of reasonable estimation.

Acknowledgements

The authors are grateful to Luiz Gonzaga Rios Filho for generation of the curve and respective analytical curvature values. Júlia Sawaki Tanaka thanks CAPES for financial help. Edson Tadeu Monteiro Manoel expresses his gratitute to CNPq/PIBIC for financial help. Luciano da Fontoura Costa is thankful the FAPESP (Procs 94/3536-6 and 94/4691-5) and the CNPq (Proc 301422/92-3) for financial support.

References

[1] D.P. Andrews, A.K. Butcher and B.R. Buckley. Acuities for spatial arrangement in line figures: human and ideal observers compared, *Vision Research*, 13:599-620, 1973.

[2] C. Blakemore and R. Over. Curvature detectors in human vision?, *Perception*, 3:3-7, 1974.

[3] R.C. Coelho and L. da F. Costa. On the application of the Bouligand-Minkowski fractal dimension for shape characterization, *Applied Signal Processing*, 3:163-176, 1996.

[4] L. da F. Costa, R.M. Cesar Jr., R.C. Coelho and J.S. Tanaka. Analysis and synthesis of morphologically realistic neural networks, in

Modeling in the Neurosciences: From Ionic Channels to Neural Networks, edited by Roman R. Poznanski, Gordon and Breach Science Publishers, p.505-527, 1999.

[5] L. da F. Costa, E.T.M. Manoel and J.S. Tanaka. A new model for neural curvature detection and its investigation in terms of neuromorphometric measures, *Proceedings of I International Seminar on Bioelectronic Interfaces and III Workshop on Cybernetic Vision*, Campinas-SP, Brazil, p.18-24, 1999.

[6] L. da F. Costa and L.A. Consularo. The dynamics of biological evolution and the importance of spatial relations and shapes, in *Human and Machine Perception 2*, edited by Virginio Cantoni et al, Kluwer Academic/ Plenum Publishers, New York, p.1-14, 1999.

[7] L. da F. Costa, L.G. Rios-Filho, J.S. Tanaka and E.T.M. Manoel. On neuronal shape and function: two case examples, in *Biophysical Neural Networks: Analytical Approaches to Neuronal Function*, edited by Roman R. Poznanski, Liebert, Inc. Publishers, New York (*in press*).

[8] A. Dobbins, S.W. Zucker and M.S. Cynader. Endstopping and curvature, *Vision Research*, 29(10):1371-1387, 1989.

[9] M. Fahle. Curvature detection in the visual-field and a possible physiological correlate, *Experimental Brain Research*, 63(1):113-124, 1986.

[10] S.T. Freeman and E.H. Adelson. The design and use of steerable filters, *IEEE Transactions on Pattern Analysis and Machine Intelligence*, 13(9):891-906, 1991.

[11] E. Haan. Edge-curvature discriminability argues against explicit curvature detectors, *Journal of Optical Society of America A*, 12(2):202-213, 1995.

[12] C. Koch and I. Segev. *Methods in Neuronal Modeling*, The MIT Press, 1995.

[13] S.R. Leiky and T.J. Sejnowski. Neural network model of visual cortex for determining surface curvature from images of shaded surfaces, *Proceedings of Royal Society of London B*, 240:251-278, 1990.

[14] J. Ogilvie and E. Daicar. The perception of curvature, *Canadian Journal of Psychology*, 21:521-525, 1967.

[15] L.A. Riggs. Curvature as a feature of pattern vision, *Science*, 181:1070-1072, 1973.

[16] B.N. Timney and C. Macdonald. Are curves detected by curvature detectors?, *Perception*, 7(1):51-64, 1978.

[17] M. Versavel, G.A. Orban and L. Lagae. Responses of visual cortical-neurons to curved stimuli and chevrons, *Vision Research*, 30(2):235-248, 1990.

[18] R.J. Watt. Further evidence concerning the analysis of curvature in human foveal vision, *Vision Research*, 24:251-253, 1984.

[19] D. Whitaker and P.V. McGraw. Geometric representation of the mechanisms underlying human curvature detection, *Vision Research*, 38:3843-3848, 1998.

[20] H.R. Wilson and W.A. Richards. Mechanisms of contour curvature discrimination, *Journal of Optical Society of America A*, 6(1):106-115, 1989.